RESEARCH ARTICLE

ADVANCED FUNCTIONAL MATERIALS
www.afm-journal.de

Searching Materials Space for Hydride Superconductors at Ambient Pressure

Tiago F. T. Cerqueira, Yue-Wen Fang, Ion Errea, Antonio Sanna, and Miguel A. L. Marques**

A machine-learning-assisted approach is employed to search for superconducting hydrides under ambient pressure within an extensive dataset comprising over 150 000 compounds. The investigation yields ≈50 systems with transition temperatures surpassing 20 K, and some even reaching above 70 K. These compounds have very different crystal structures, with different dimensionality, chemical composition, stoichiometry, and arrangement of the hydrogens. Interestingly, most of these systems display slight thermodynamic instability, implying that their synthesis will re quire conditions beyond ambient equilibrium. Moreover, a consistent chemical composition is found in the majority of these systems, which combines alkali or alkali-earth elements with noble metals. This observation suggests a promising avenue for future experimental investigations into high-temperature superconductivity within hydrides at ambient pressure.

1. Introduction

A superconductor is a material exhibiting zero electrical resistance and perfect diamagnetism when cooled below a critical temperature T_c. Such unique properties have paved the way for groundbreaking applications of superconductors, ranging from powerful magnets in medical imaging, particle accelerators, or fusion reactors to superconducting qubits in quantum computers. Since the discovery of superconductivity in Hg in 1911, research on this field has focused on increasing T_c, with particular emphasis on achieving high T_c values above the boiling point of nitrogen (77 K). Nowadays, one of the primary goals in physics remains to find materials that exhibit superconductivity at ambient conditions to unlock new fundamental physics and enable wide applications of superconductors.

In the so-called unconventional superconductors, showcased by cuprate compounds, the highest superconducting transition temperatures are 134 and 164 K at ambient pressure and 30 GPa, respectively.[1] Nevertheless, owing to the lack of a distinct understanding of the pairing mechanism, there is at the moment no quantitative theory that can be used to predict the superconducting properties of such systems, seriously hampering the search for new unconventional compounds. On the other hand, the theoretical prediction and characterization of conventional superconductors, where the electrons at the Fermi surface are coupled by phonons to form Cooper pairs, can be well addressed by a combination of ab initio studies and Eliashberg theory. Unfortunately, since the experimental observation of superconductivity in MgB_2 in 2001,[2] its T_c of 39 K remains the highest among the ambient-pressure conventional superconductors.

In the theory of electron–phonon coupled superconductors, the critical temperature T_c is proportional to the Debye temperature θ_D. Hydrogen, being the lightest element, provides a high

T. F. T. Cerqueira
CFisUC
Department of Physics
University of Coimbra
Rua Larga, 3004-516 Coimbra, Portugal

Y.-W. Fang, I. Errea
Fisika Aplikatua Saila
Gipuzkoako Ingeniaritza Eskola
University of the Basque Country (UPV/EHU)
Europa Plaza 1, 20018 Donostia-San Sebastián, Spain

The ORCID identification number(s) for the author(s) of this article can be found under https://doi.org/10.1002/adfm.202404043

DOI: 10.1002/adfm.202404043

Y.-W. Fang, I. Errea
Centro de Física de Materiales (CSIC-UPV/EHU)
Manuel de Lardizabal Pasealekua 5, 20018 Donostia-San Sebastián, Spain

I. Errea
Donostia International Physics Center (DIPC)
Manuel de Lardizabal Pasealekua 4, 20018 Donostia-San Sebastián, Spain

A. Sanna
Max-Planck-Institut für Mikrostrukturphysik
Weinberg 2, D-06120 Halle, Germany
E-mail: sanna@mpi-halle.mpg.de

M. A. L. Marques
Research Center Future Energy Materials and Systems of the University Alliance Ruhr and Interdisciplinary Centre for Advanced Materials Simulation
Ruhr University Bochum
Universitätsstraße 150, D-44801 Bochum, Germany
E-mail: miguel.marques@rub.de

Debye temperature to the compounds that it forms, making hydrides the most obvious choice in the search for conventional high T_c superconductors.[3] Over the past two decades, hundreds of binary hydrides, covering the majority of the chemical elements in the periodic table, have been either theoretically predicted or experimentally observed to exhibit superconductivity. However, in spite of chemical pre-compression in hydrides, experimental results indicate that achieving high T_c superconductivity still requires large external pressures. For example, experiments have suggested that $T_c > 200$ K generally requires pressures exceeding 150 GPa: T_c of 250 K in LaH_{10} at 150 GPa,[4,5] T_c of 215 K in CaH_6 at 172 GPa,[6] and T_c of 243 K in YH_9 at 201 GPa,[7] to name a few examples.

Recently, the search for high T_c hydrides useful for device applications, has shifted from solely prioritizing the enhancement of T_c to achieving high T_c materials at low or even ambient pressure. Unfortunately, only a few superconducting binary hydrides have been found in ambient-pressure experiments, and their critical temperatures are below or near 10 K, for instance PdH with T_c of 9 K,[8] $TiH_{0.71}$ with T_c of 4.3 K,[9] $MoH_{1.2}$ with T_c of just 0.92 K,[10] Th_4H_{15} with T_c of 8.2 K,[11] $NbH_{x<0.7}$ with T_c of 9.4 K,[12] and ZrH_3 with T_c of 11.6 K.[13] All these experimental studies (except the case of ZrH_3) were carried out more than 30 years ago.

Compared to the binary hydrides, the ternary, or more generally, the multinary hydrides have a much larger structural phase space and are therefore expected to host higher T_cs at low and ambient pressures.[14,15] There were several experimental studies in the 1970s in ternary hydrides such as HfV_2H with a T_c of 4.8 K[16] and $Pd_{0.55}Cu_{0.45}H_{0.7}$ with a T_c of 16.6 K.[17] However, more recently, theoretical reports that are facilitated by high-throughput calculations, high T_c templates, crystal structure prediction, or machine learning methods, have pioneered the exploration of promising superconducting hydrides at low/ambient pressure. Due to the strong quantum ionic and anharmonic effects, both $BaSiH_8$[18] and LuN_4H_{11}[19] are predicted to exhibit dynamical stability and high T_c of 94 and 100 K, respectively, at 20 GPa. The compound $CsBH_5$ is predicted to have a strong electron–phonon coupling constant λ of 3.96 at 1 GPa, resulting in a high T_c of 83 K.[20] The deep-learning-recommended MgBH[21] and the perovskite $MgHCu_3$[22] are predicted by electron-phonon coupling calculations to show T_c values of 15.5 and 42 K at atmospheric pressure, respectively. Finally, Mg_2IrH_6 with a T_c above 80 K was predicted, together with other compounds with the same cubic structure, in our recent study[23] and in Ref. [24].

Herein, we use a machine-learning method to accelerate the search of superconductivity in a dataset of more than 150 000 hydrides. Our workflow has identified 54 compounds with T_c exceeding 20 K, most of which have not been reported previously. These results provide a huge platform for ambient-pressure superconducting hydrides, inviting worldwide experimental groups to explore their synthesis, and further study the transport properties, Meissner effect, isotope effect and potential device applications.

2. Results and Discussion

Here we are concerned with hydrides only. To identify such compounds, that are potentially high-temperature conventional superconductors at ambient pressure, we used a machine learning accelerated workflow along the lines of Ref. [25]. Unfortunately, the dataset of Ref. [25] did not include any high-temperature hydride (with the exception of PdH which has a too-high T_c in the harmonic approximation), so the machine trained in this dataset had difficulties predicting hydrides. To circumvent this problem, we added manually a series of hydrides to the dataset and retrained the machine, which was subsequently used to predict the superconducting properties of the hydrides present in the ALEXANDRIA database.[25,26] This workflow consists of three main steps: 1) a machine learning model provides a first crude (but extremely fast) pruning of the data, filtering out materials that are unlikely to show high T_c 2) compounds predicted to have T_c above 20 K are then analyzed with density-functional perturbation theory (DFPT) and added to the dataset, while materials showing imaginary phonon frequencies are discarded 3) a set of very accurate calculations are performed for the most promising materials using state-of-the-art first principle methods. We note that step 2) validates 1) and 3) validates 2), allowing for the identification of the false positives. Eventual false positives resulting from incorrect machine learning predictions that are not captured by retraining the model are, unfortunately, overlooked. Our final model had an error of 1.93 K for T_c, 22.47 K for ω_{log}, and 0.16 for λ. This should be compared to the average values in the training set of 3.41 K, 233.38 K, and 0.48, respectively.

In **Tables 1** and **2** we present all the hydrides predicted to have superconducting transition temperatures above 20 K (see Supporting Information for extra details for each compound). We note that the values presented in the tables are the ones obtained with density-functional perturbation theory and the Allen–Dynes formula, and not the values predicted by the machine-learning model. We divided the compounds by families, and ordered by T_c, in order to facilitate the analysis. As we can see, many compounds belong to just a few families such as the SM_2-TM-H_6 family,[23,27] perovskites (both normal and inverted), and double perovskites. There is also a striking regularity in what concerns the chemical compositions. In fact, the large majority of the hydrides include both a simple metal (SM), typically an alkali, alkali earth, or even a IIIA or IVA element, and a transition (TM) or noble metal.

2.1. SM_2-TM-H_6

Four elements of the SM_2-TM-H_6 family have already been discussed in Ref. [23], namely Mg_2RhH_6, Mg_2IrH_6, Mg_2PdH_6, Mg_2PtH_6, and a few more were proposed in Ref. [27]. This structure, depicted in **Figure 1a**, is described by a face-centered cubic lattice with space group $Fm\bar{3}m$. Here, the SM atoms are in the 8c, the TM atoms in the 4a, and the H atoms in the 24e Wyckoff positions. As we can see from Figure 1a, the H atoms form isolated octahedra around the TM atoms. All high-temperature superconductors we found within this family were perfectly symmetric and did not exhibit any deformation of the octahedra.

From the chemical point of view, in all our systems SM is a simple metal from groups IA, IIA, or IIIA while TM is a transition or a noble metal (see Table 1). It is simple to understand the chemical compositions in Table 1 by a simple electron counting argument. The parent compound of this family, Mg_2RuH_6,[29,30] is a stable semiconductor. Considering the standard oxidation

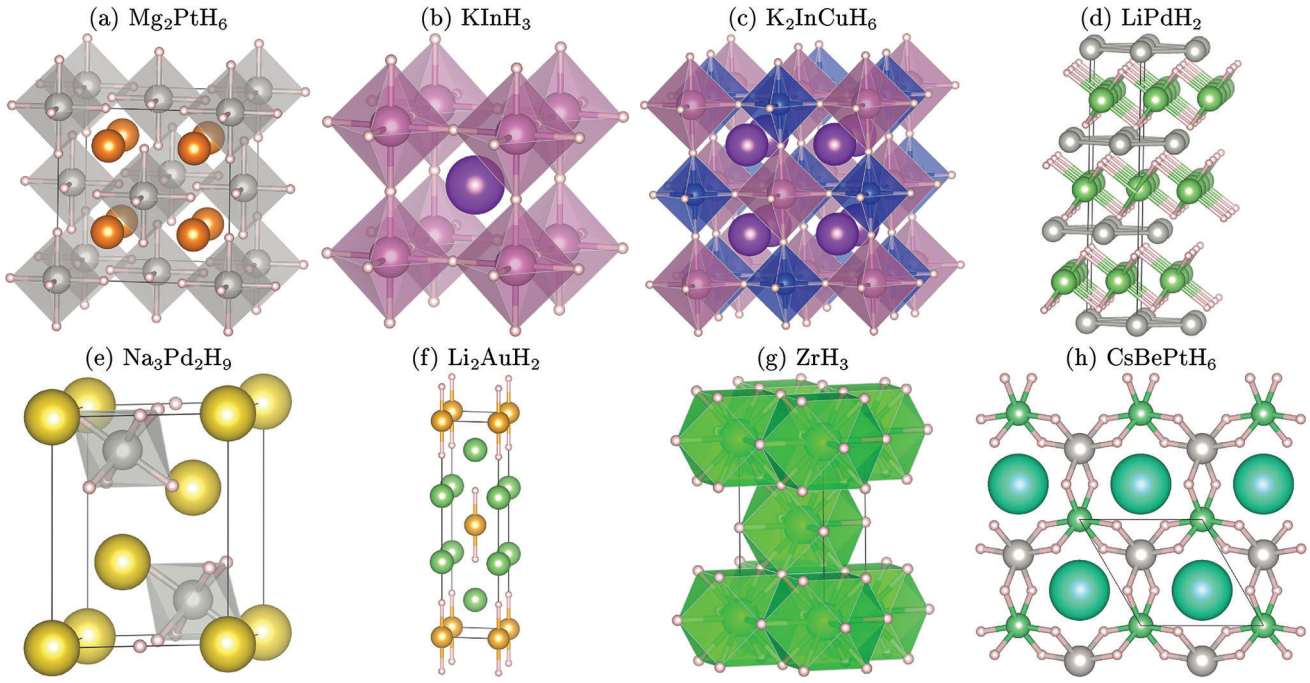

Figure 1. Crystal structures of selected hydrides. The lines indicate the conventional cell. In the pictures H atoms are white, Li and Be green, Na yellow, Mg orange, K violet, Cu dark blue, Zr green, In pink, Cs cyan, Pd and Pt grey, and Au orange.

states of +2 for Mg and –1 for H in hydrides, this leads to +2 for Ru, a standard oxidation state found in this metal (although less common than the +3 or +4 states). In total, this compound has 18 valence electrons that fill completely the electronic valence states. A superconducting state emerges when this compound is doped with electrons, either one per formula unit (e.g., Mg_2IrH_6, Al_2TcH_6, or Na_2AuH_6) or two per formula unit (e.g., Mg_2PtH_6 or Ga_2RuH_6).

From the electronic point of view, all compounds with SM being an alkali or an alkali earth are quite similar. The SM atom is fully ionized, so the top of the valence bands and the bottom of the conduction bands [31] are dominated by H and TM states. There are, of course, some changes to the dispersion of the bands that are system-specific, leading to different densities of states at the Fermi level, even for compounds that are isoelectronic. The situation is slightly more complicated when the SM is a group IIIA metal, as its states are not entirely ionized. This leads to an entirely different dispersion of the bands and therefore a different Fermi surface. In spite of this, the superconducting properties are in line with the ones of the IA and IIA-based compounds.

Concerning the phonon dispersions (see Supporting Information), the low energy modes are usually dominated by the TM atom, as expected by their larger mass, followed by a manifold composed mainly by the SM atom. However, in some cases where SM is a group IIIA metal, we see a strong mixture of SM and TM states in the low energy range (e.g., in Al_2TcH_6 or in Al_2ReH_6). The higher energy states, that contribute mostly to λ are dominated by the vibrations of the hydrogen octahedra. The maximum phonon frequencies present in the spectrum can go from ≈125 to almost 240 meV, depending on the chemical composition.

These compounds exhibit a wide range of values for ω_{log} with the lowest being 292 K (Ga_2RuH_6) up to more than 770 K (Mg_2PtH_6 and Mg_2RhH_6). On the other hand, the values of the electron-phonon coupling constant are typically ≈1–1.2. Exceptions to this are Ga_2RuH_6, which has a very soft mode at the X-point (that is also responsible for the abnormally low value of ω_{log} for this compound), and Mg_2NiH_6 which has the low-value $\lambda = 0.61$ (partially compensated by the high value of $\omega_{log} = 921$ K). The combination of high ω_{log} and relatively high λ allows for dynamically stable crystals with the very high values of T_c present in Table 1.

For the materials of this family with distances to the hull below 100 meV per atom, we performed ab initio molecular dynamics simulations in order to analyze their kinetic stability. The results did not show any phase transition up to 150 K with suggests the stability of these materials at temperatures above their T_c (see Supporting Information).

2.2. Perovskites

Concerning the hydride perovskites, we find both normal (see Figure 1b) and inverted systems. There are a series of hydride perovskites that have been synthesized experimentally.[32] Many of these are charge compensated, often combining an alkali and an alkali earth in positions 1a and 1b, such as $LiBeH_3$,[33] $BaLiH_3$,[34] or $KMgH_3$.[35] Not surprisingly, such systems are semiconducting. There are, however, a few non-charge compensated systems that have been discovered, such as $AlSrH_3$[36] (obtained through a high-pressure synthesis procedure) or $SrPdH_{2.7}$.[37] There are also a few inverted (anti-)perovskites reported in the experimental literature, such as $ChHM_3$ where M = Li, Na, and Ch is a chalcogen[38] or $InH_{0.8}Pd_3$.[39]

The band structure of $KInH_3$ has a characteristic very dispersive, parabolic band centered at R that crosses the Fermi level. All

Table 1. Superconducting transition temperatures calculated with the Allen-Dynes formula (T_c^{AD} in K), logarithmic average of the phonon frequencies (ω_{log} in K), average of the square of the phonon frequencies (ω^2 in K), electron–phonon coupling constant (λ) and distance to the convex hull of stability (E_{hull} in meV per atom). The first column of the table contains a running number that can be used to identify the compounds in the Supporting Information.

#		T_c^{AD}	ω_{log}	ω^2	λ	E_{hull}	Comment
SM_2-TM-H_6[27]							
1	Li_2CuH_6	86.0	491	890	1.96	171	
2	Mg_2PtH_6	78.3	770	922	1.24	140	[23]
3	Mg_2PdH_6	63.8	760	911	1.08	120	[23]
4	Mg_2IrH_6	59.4	634	1052	1.16	61	[23]
5	Mg_2RhH_6	53.8	771	1132	0.96	30	[23]
6	Na_2AgH_6	46.1	511	1000	1.12	204	
7	Al_2MnH_6	43.9	587	1014	1.00	68	
8	Al_2TcH_6	43.1	484	964	1.11	53	
9	Al_2ReH_6	36.4	505	994	0.98	55	
10	Ca_2AgH_6	35.9	418	740	1.09	166	
11	Ca_2LiH_6	33.0	433	706	1.01	226	
12	Na_2AuH_6	31.6	632	1196	0.80	73	
13	Na_2CuH_6	29.4	580	1122	0.81	135	
14	Ga_2RuH_6	26.9	292	822	1.14	230	
15	Mg_2NiH_6	22.7	921	1120	0.61	63	
16	Ga_2OsH_6	20.9	262	841	1.04	179	
Perovskites							
17	$KInH_3$	72.9	487	698	1.70	77	
18	Al_4H	30.4	430	546	0.97	136	[28]
19	$AlHgH_3$	28.4	403	854	0.96	278	
20	$PbHgH_3$	25.8	462	808	0.85	420	
21	$PbOsH_3$	23.2	292	722	1.03	369	
22	$TiHMg_3$	21.8	196	362	1.31	370	inverted
Double Perovskites							
23	K_2InCuH_6	53.0	510	716	1.25	47	
24	K_2LiCuH_6	47.1	470	719	1.21	116	
25	Na_2LiCuH_6	45.9	666	950	0.95	102	
26	Na_2SiPdH_6	39.8	875	1062	0.77	84	
27	Na_2LiZnH_6	37.8	519	763	0.98	146	
28	Na_2GaRuH_6	35.2	535	864	0.93	162	
29	Cs_2NaSnH_6	34.5	324	588	1.27	67	
30	K_2AlHgH_6	32.5	349	701	1.15	86	
31	K_2HgAuH_6	32.5	396	913	1.06	49	
32	K_2InAgH_6	31.7	660	860	0.79	32	
33	Rb_2AlHgH_6	31.4	140	463	2.53	83	
34	Na_2CdCuH_6	26.0	740	986	0.69	63	
35	Na_2MgCuH_6	24.7	251	707	1.20	92	
36	Pb_2CuRuH_6	23.7	243	712	1.19	149	
37	K_2AlCdH_6	21.0	507	834	0.74	74	

other hydride perovskites have very diverse electronic band structures and Fermi surfaces. We note due to the high Fermi velocity of the bands, the density of electronic states at the Fermi level is not extremely high in most cases. The low-energy phonons of the normal hydride perovskites are as expected dominated by the heavier atoms, but have a sizeable contribution to λ. In many of these systems, H modes are highly dispersive and can be found ≈30–180 meV. The inverted perovskite has a very different phonon dispersion: in $TiHMg_3$ the H-modes are lower in energy and are more dispersive, almost touching the low-energy Ti–Mg modes, and contribute significantly to the binding of the Cooper pairs.

Values of ω_{log} for the normal perovskites are not particularly large and are found in the range of 40–60 meV. This is however compensated by rather large values of λ that can reach 1.70 for $KInH_3$. In the inverted perovskite, the situation is similar, but with even lower values of ω_{log}. Finally, we would like to mention Al_4H, a material proposed in Ref. [28] where Al occupies both the 1b and 3d Wyckoff positions of the cubic perovskite structure.

Table 2. Continuation of Table 1.

#		T_c^{AD}	ω_{log}	ω^2	λ	E_{hull}	comment
Other structures							
38	Be_8H	65.9	588	718	1.34	202	[43]
39	Mg_2SrPtH_8	49.4	568	925	1.10	117	
40	Mg_2SrPdH_8	49.1	652	925	1.00	93	
41	Mg_2BaPdH_8	41.6	646	939	0.92	63	
42	Mg_2BaPtH_8	38.4	590	961	0.92	102	
43	Na_2AuH_4	43.8	394	598	1.31	35	
44	$LiPdH_2$	38.6	532	849	0.98	108	[44]
45	$NaPdH_3$	29.3	215	722	1.56	193	
46	$Na_3Pd_2H_9$	25.3	516	1031	0.80	86	
47	Li_2AuH_2	20.8	368	762	0.86	59	
48	Li_4BeH_5	37.2	465	716	1.04	154	
49	PdH	34.9	343	429	1.24	8	[8,45]
50	InH	31.2	312	724	1.20	223	
51	ZrH_3	25.8	363	748	0.97	105	[13]
52	InH_3	20.6	218	700	1.17	286	
53	Zr_2HfH_8	25.1	266	663	1.16	94	
54	$KBePtH_6$	39.9	371	764	1.27	138	
55	$RbBePtH_6$	37.9	379	767	1.21	135	
56	$CsBePtH_6$	30.9	370	787	1.07	130	
57	Li_2CuGaH_6	37.9	527	891	0.97	133	
58	K_2AgCdH_6	27.5	422	775	0.92	75	
59	Na_2PdIrH_6	23.5	456	736	0.82	93	

2.3. Double Perovskites

In view of the number of normal perovskites we found, it is not surprising that several double perovskite systems (see Figure 1c) also appeared in our survey. From Table 1 we see that the 8c position (the counterpart of the 1a position of the ternary perovskites) is mostly occupied by an alkali (with the exception of Pb_2CuRuH_6), while the 4a and 4b positions include two cations, often combining a SM with a TM. Of course, the quaternary system allows for a much larger number of chemical compositions than the ternary one.

To our knowledge, there are no experimentally synthesized hydride double perovskites. However, these systems have been proposed theoretically as high-temperature ferromagnetic

semiconductors[40] and the effect of strain on the hydrogen storage characteristics in K_2NaAlH_6 has been studied in Ref. [41].

What is perhaps surprising is the diversity of electronic band structures and of Fermi surfaces for the double perovskites of Table 1. In all cases with an alkali in 8c position, these atoms are fully ionized and do not contribute to the density of states at the Fermi level. The Fermi level, instead, contains states of H and of the cations in positions 4a and 4b. The chemical diversity of these ions, with some having *d* states and others not, leads to different band structures close to the Fermi level. From this we can conclude that the detailed shape of the Fermi surface or the Fermi velocity are not determinant factors for the superconducting properties of double perovskite hydrides, but only the contribution of H to the density of states at the Fermi level.[42] The same holds true for the phonon band structure. Although the cations in the 4a and 4b positions are normally responsible for the acoustic and low-lying optical modes, the higher-lying optical modes show a variety of dispersions and frequencies. The highest optical mode is usually in the range of 135–175 K.

We can see from Table 1 that values of λ are between 0.7–1.25, while $\omega_{\log}$ is between 250 and 875 K. These compounds show extremely well that the highest T_c is obtained through the synergy between λ and $\omega_{\log}$, and not by extreme values of either quantity. We emphasize that in none of the normal, inverted, or double perovskites we encounter any rotation or tilting of the octahedra that are so common in oxide perovskites.

2.4. Other Compounds

From the compounds in Table 2, the one with the highest predicted T_c is Be_8H. This material, proposed as a high-temperature superconductor in Ref. [43] is composed by double triangular layers of Be intercalated with triangular layers of H. It has a complicated band structure, with different bands crossing the Fermi energy. Interestingly, the large value of $\lambda = 1.34$ is mainly due to the lowest-lying optical modes of Be, although with a non-negligible contribution of the three high-frequency modes composed mostly of H vibrations.

We then encounter four closely related systems, specifically $Mg_2\{Sr, Ba\}\{Pt, Pd\}H_8$ with predicted transition temperatures of ≈49 K (for the Sr compounds) and 40 K for the Ba compounds. These crystallize on a trigonal phase with alternating layers of $Mg_2\{Pt, Pd\}H_6$ and $\{Sr, Ba\}H_2$. We find two bands crossing the Fermi surface, with one of the crossings (at the H point) exactly at the Fermi energy. Due to the difference in atomic masses, the phonon frequencies are well separated, with the acoustic and lowest-lying optical branches with {Sr, Ba} and {Pt, Pd} character, followed by modes with mostly Mg character. Finally, the H vibrations form two separated manifolds at higher energy spanning frequencies from 40 to 140 meV. The electron-phonon coupling constants for these materials are $\approx\lambda = 1$, but $\omega_{\log}$ has large values of ≈600–650 K.

With transition temperatures between 20 and 44 K we find a series of systems with similar chemistry, specifically with compositions involving one light alkali metal (Li or Na) and one noble metal (Au or Pd, see examples in Figure 1d–f). The one with the highest transition temperature is Na_2AuH_4, a tetragonal compound with alternating layers of Na and AuH_4. In the latter compound, the H atoms form the vertices of isolated squares aligned with the direction of the layer, with the Au atoms at the center of the squares. There are two bands crossing the Fermi surface, with a Dirac band crossing at the Fermi energy at a point between X and Σ. The relatively high T_c is mostly due to the electrons with the lowest-lying H-modes at ≈40 meV.

The next compound, $LiPdH_2$ has delafossite structure with PdH_2 layers intercalated with Li (see Figure 1d). This material, with a predicted T_c of almost 40 K has already been discussed in Ref. [44]. Next, come two Na-Pd hydrides, with very different stoichiometries, structures, and superconducting properties, but with similar T_c. The first, $NaPdH_3$, is cubic, with sharing PdH_6 octahedra tilted with respect to each other, with all H atoms shared between two octahedra. The second, $Na_3Pd_2H_9$ has aligned PdH_6 octahedra that form chains through the sharing of two H per octahedron (see Figure 1e). These two compounds exhibit very different band structures: the first has many bands crossing the Fermi surface, leading to a complicated Fermi surface; the second has two bands at the Fermi level, with several crossings at, or near, the Fermi energy. Both compounds have phonons arranged in three well-separated manifolds with comparable energies, with the acoustic and low-lying optical branches with Pd–Na character, and the two higher-lying manifolds due to H-vibrations of the octahedra. Finally, Li_2AuH_2 has a very interesting structure, with AuH_2 linear units alternating with layers of Li. The values of $\lambda = 0.86$ and $\omega_{\log} = 368$ K are relatively modest for the hydrides in this list, leading to a $T_c \approx 20$ K.

The structure of Li_4BeH_5 is very interesting, with the Li atoms forming a snub-square lattice[46] when viewed from the *c*-axis. There are two electronic bands crossing the Fermi surface, one with high Fermi velocity while the other forms a pocket around the *M*-point. The Fermi level lies on a steep shoulder of the density-of-states, suggesting the T_c could be increased by electron doping. The phonon branches contributing the most to λ are the lower-lying modes, where one sees a strong mixture of Li, Be, and H modes.

Next in Table 2 comes a series of simple transition metal hydrides with T_c in the range of 20–35 K. PdH is a well-known superconductor[8] where anharmonic effects have a huge effect in decreasing the transition temperature.[45] On the other hand, ZrH_3 (see Figure 1g) has been recently reported with a T_c = 11.6 K.[13] We also find two indium hydrides: the rather thermodynamically unstable InH has a very simple hexagonal structure with two atoms in the unit cell. There are two very dispersive bands crossing the Fermi surface, leading to a relatively low density of states at the Fermi surface. Indium and hydrogen phonons are well separated, with the three acoustic (indium) and the first and second optical (hydrogen) branches contributing the most to λ. Finally, Zr_2HfH_8 has a curious crystal structure that has the form of a Triakis triangular tiling, with {Zr, Hf} in the hexagonal positions when viewed from the *a*-axis. Of course, due to the similarity between Zr and Hf we can expect a certain amount of alloying in the cation positions. The Fermi surface is quite complicated, with many bands crossing the Fermi surface, and the Fermi level lies on the steep shoulder of the density of states. Most of the value of $\lambda = 1.16$ comes from the lowest manifold of phonon bands composed exclusively of Zr and Hf vibrations and from the lowest hydrogen vibrations, while the higher optical hydrogen modes couple very weakly to the electrons.

The three compounds {K, Rb, Cs}$BePtH_8$ have a hexagonal structure, with $BePtH_8$ layers intercalated by alkali layers (see Figure 1h). The band structure close to the Fermi level is essentially determined by the $BePtH_8$ layers. These are characteristic of an indirect band gap semiconductor with heavy holes and light electrons. The extra electron donated by the alkali atom half-fills the conduction band leading to a metallic ground-state. The strong electron–phonon coupling constants $\lambda = 1.07–1.27$ are mainly due to vibrations of the heavy atoms and the lowest-lying hybridized Be–H modes. We also see that ω_{log} is basically independent of the alkali, while λ decreases going from K to Cs, leading to a decrease of T_c.

Finally, we find three systems, Li_2CuGaH_6, K_2AgCdH_6, and Na_2PdIrH_6 with similar chemical compositions, but different crystal structures and electronic and phononic band structures. In spite of this, they all have similar values of λ and ω_{log}, leading to T_c between 23 and 37 K.

2.5. Statistical Analysis

These examples show that there is not a unique or simple recipe linked to strong superconductivity in hydrides at ambient pressures. However, we can see some patterns from a statistical analysis of our dataset. In **Figure 2**a we analyze the correlation between the thermodynamic stability and T_c. This figure is obtained by grouping the materials according to their energy from the hull and, for each group, computing the histogram of T_c values (i.e., the number of materials in the figure is normalized column-wise). The figure shows that, while there is not a direct proportionality between T_c and thermodynamic stability, the chance of finding high T_c outliers increases significantly with the distance from the hull. We identify two regions (separated by a dashed line): a high T_c zone where materials are rare ("[1]" in the Figure) and a low-T_c zone with a high density of materials ("[2]" in Figure). Ideally we would be interested in high T_c stable materials, but this set appears to be rather empty. Therefore the sparse region of high stability and high T_c is the most promising search domain.

A second aspect that emerges from our analysis is the complex relation between hydrogen and superconductivity. As shown in Figure 2c there is a correlation between high hydrogen content at the Fermi level (as measured by computing the H fraction of the density of states) and T_c. High hydrogen content is linked (as it should be)[3,42] to higher values of T_c (region "[1]" in Figure 2c. Unfortunately, the high hydrogen content also correlates with thermodynamic instability. As shown in Figure 2b, by increasing the H content the center of mass of the material distribution shifts toward higher energy (region "[1]" of the plot). Note that the data are normalized row-wise. From this figure it is clear that the region of interest is in materials for which the Fermi density of states is dominated by the host chemical composition and the H contribution is less than 50% of the total. This region is indicated by the label "[2]" in Figure 2b,c.

2.6. Analysis of Selected Hydrides

Among the superconducting hydrides predicted in our high-throughput search we have selected a small set of compounds

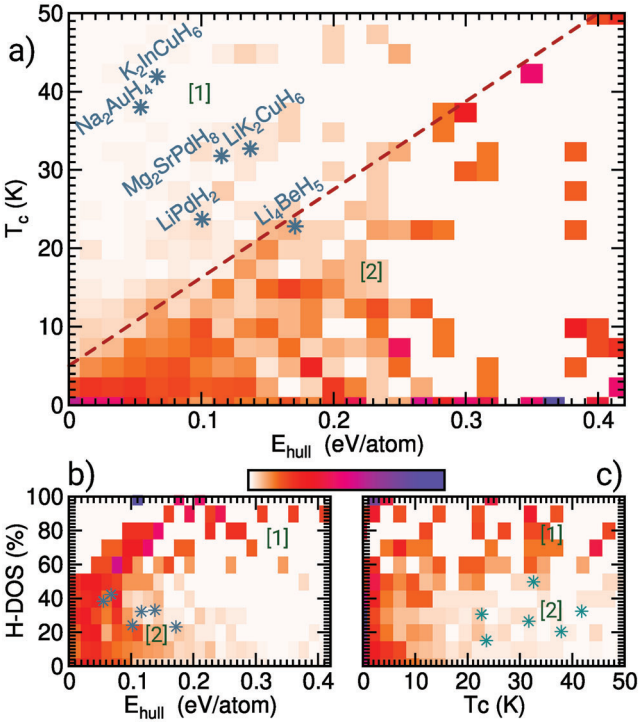

Figure 2. Analysis of superconducting hydrides: a) Histogram of T_c as a function of the distance to the convex hull. The dashed line is a guide to the eye marking a threshold in critical temperature separating high from low probability regions. The histogram is normalized column-wise and a color-bar (white to blue) indicates the normalized histogram height. b) Relation between the distance do the convex hull and the hydrogen contribution to the density of states at the Fermi level. c) Relation between T_c and the hydrogen contribution to the density of states at the Fermi level. The histograms in (b) and (c) are normalized row-wise. Stars show some of the materials discussed in Section 2.6.

and investigated these with higher accuracy and in further detail. There are two main problems we want to address here: 1) The high density of states at the Fermi level of these compounds, and the fact that the Fermi level is often at a steep shoulder or a peak, which makes the convergence with respect to smearing and k-points very complicated. 2) The replacement of the Coulomb interaction by the number μ^* that is given a rather arbitrary value (usually ≈0.10) is hardly justified for many of the high T_c hydrides.[47–49] Instead, the full energy dependence of the Coulomb term should be maintained in the calculation of the superconducting properties.

The list of compounds that we selected, together with some of their properties are collected in **Table 3**, which includes four materials Mg_2XH_6 with X = Rh, Pd, Ir, Pt already discussed in Ref. [23]. These are outlier materials with respect to the general trends discussed in the previous section, close to the hull of stability and with high T_c. First, we observe that the calculated T_cs reported in Table 3 are in most cases lower than that listed in Table 1 and Table 2. In some cases, such as $LiPdH_2$ and Mg_2SrPdH_8, the difference is related to changes in the estimated e-ph coupling parameters (owing to the increased numerical accuracy), however, in most of the cases the e-ph coupling is confirmed and the lower T_c stems from a strong Coulomb repulsion, which here we compute from first principles.

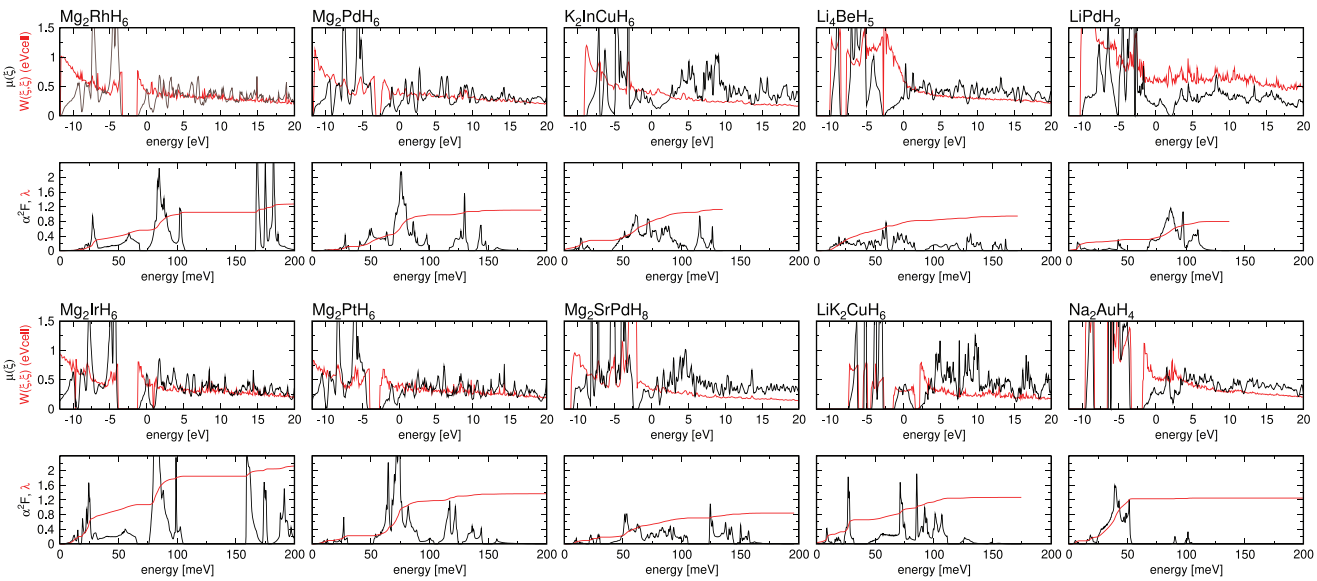

Figure 3. Coupling parameters entering the isotropic Eliashberg equations.[53,54] The quantity $W(\xi, \xi')$ is the Coulomb interaction computed in the random phase approximation, $\mu(\xi) := W(\xi, \xi)N(\xi)$ is the product of W and the density of electronic states. Finally, $\alpha^2F(\omega)$ is the Eliashberg electron–phonon function, $\lambda(\omega) := 2\int_0^{\omega} \frac{\alpha^2F(w)}{w} dw$ is the coupling integration curve.[49] The colors of the plotted lines in each panel correspond to the labels on the vertical axes.

Table 3. Electron–phonon coupling constant λ, logarithmic average of the phonon frequencies ω_{log} (in K), density of states at the Fermi level N_F (in (eV cell)$^{-1}$), the H content at the Fermi level (%), the Coulomb potential μ, transition temperatures T_c (in K) and superconducting gaps Δ (in meV) for the twelve compounds reported here. Calculations were performed with the isotropic Eliashberg equations including full ab initio Coulomb interactions.

	λ	ω_{log}	N_F	H%	μ	T_c	Δ
Mg_2RhH_6	1.3	766	2.32	18.4	0.45	48.5	8.4
Mg_2PdH_6	1.1	754	0.80	28.3	0.17	66.5	11.2
Mg_2IrH_6	2.13	581	2.90	15.2	0.58	77.0	16.3
Mg_2PtH_6	1.4	696	1.03	22.6	0.20	80.4	15.0
K_2InCuH_6	1.14	448	1.38	32.2	0.26	41.9	7.0
K_2LiCuH_6	1.28	354	2.34	49.6	0.35	32.7	5.6
Mg_2SrPdH_8	0.84	608	1.10	26.3	0.19	31.8	5.1
Na_2AuH_4	1.28	391	1.09	20.2	0.27	38.0	6.6
$LiPdH_2$	0.80	454	0.53	14.9	0.16	23.7	3.8
Li_4BeH_5	0.95	460	1.05	30.4	0.31	22.8	3.7

The hydrogen contribution to the pairing is evident from the phonon band structure and electron–phonon coupling functions reported in **Figure 3**. In fact, more than 50% of the integrated coupling constant λ originates from pure-hydrogen phonon modes, which as we discussed above, tend to be well separated from the vibrational modes of the host elements. The only exception to this is Li_4BeH_5, where we see a low-energy region of mix-modes. In stable materials at low pressure hydrogen bonds are usually completely saturated, therefore hydrogen modes have no coupling with states at the Fermi level. What makes these hydrides quite special is that hydrogen states contribute significantly to the Fermi density of states (of the order of 25% according to atomic projections), furthermore they are not localized but strongly overlapping and hybridizing with the states of the host similar to what occurs in high-pressure superconducting hydrides.[49]

The screened coulomb interaction W (red curves in the panels in the first and third rows of Figure 3) is computed in the random phase approximation which is expected to be quite accurate for this class of materials.[50] The diagonal part of the W-function is relatively featureless, showing a nearly monotonous decrease with the band energy. This behavior, reminiscent of free electron systems, indicates that electronic states are well-screened.[50,51] However, the strength and effectiveness of the Coulomb repulsion is strongly affected by the density of states which shows a complex material dependence. The most peculiar cases are the Mg_2IrH_6 and Mg_2RhH_6 systems where the Fermi level is pinned to a peak in the density of states, leading to a complicated (and quite poor) Coulomb renormalization mechanism.[52] To a lesser extent a peak in the density of states also causes LiK_2CuH_6 to be characterized by a strong Coulomb repulsion. The other materials in the set are less problematic.

3. Conclusion

We presented a machine-learning-assisted approach to search for superconducting hydrides under ambient pressure within an extensive dataset comprising over 150 000 compounds. Our investigation yielded ≈50 systems with transition temperatures surpassing 20 K, and reaching above 70 K. These systems have a large variety of crystal structures and geometrical characteristics. However, we find a consistent chemical composition in the majority of these systems, which combines alkali or alkali-earth elements with noble metals.

On the downside, we observe that most of the systems we find, while being dynamically stable, are not on the hull of thermodynamic stability (while being close to it). This points to the fact that the experimental synthesis of our predicted compounds may require conditions beyond ambient equilibrium and skilled material engineering strategies.

A statistical analysis of our predictions, as well as in-depth theoretical characterization for a set of selected materials, provide a reasonably clear picture of the superconducting mechanism in hydrides at room pressure. The crucial aspect is that hydrogen states are present at the Fermi level, strongly hybridized with those of the host. These are delocalized (non-molecular) metallic states that are well screened and lead to large values of the density of states. In this situation, both medium or high-energy hydrogen phonon modes and low-energy host modes contribute to the coupling λ. The final value of T_c is a complex interplay of a large density of states, correct phonon energies, high hydrogen contribution to the Fermi density of states and low Coulomb repulsion. In a statistical sense, we observe that there is a direct correlation between low thermodynamic stability, high hydrogen content and high T_c. This observation suggests a promising avenue for future experimental investigations into high-temperature superconductivity within hydrides at ambient pressure.

4. Computational Methods

All density-functional perturbation theory calculations were performed using versions 6.8 and 7.1 of QUANTUM ESPRESSO[55,56] with the Perdew–Burke–Ernzerhof (PBE) for solids (PBEsol)[57] generalized gradient approximation.

Geometry optimizations were performed using uniform Γ-centered k-point grids with a density of 3000 k-points per reciprocal atom. If this resulted in an odd number of k-points in a given direction, the next even number was used instead. Convergence thresholds for energies, forces and stresses were set to 1×10^{-8} a.u., 1×10^{-6} a.u., and 5×10^{-2} kbar, respectively. For the electron–phonon coupling, a double-grid technique was employed with the k-grid used in the lattice optimization doubled in every direction as the coarse grid, and a k-grid quadrupled in each direction as the fine grid. For the q-sampling of the phonons, half of the k-point grid described above was used. The double δ-integration to obtain the Eliashberg function was performed with a Methfessel-Paxton smearing of 0.05 Ry.

Distances to the convex hull were computed using the PBEsol approximation.[57] All pertinent materials available in the Alexandria database[26,58] were considered and they were re-optimized following Ref. [59]. This set of materials included most of the experimentally known hydrides present in the Inorganic Crystal Structure Database,[60] as well as many theoretical phases. Most of the theoretical phases were constructed by analogy, substituting the metals in known hydride structures with other "similar" chemical elements. The chemical element substitutions were suggested either by a similarity scale[61] or by using machine learning models.[26] It was noted that this dataset, together with the rest of Alexandria, can be freely accessed through an optimade interface.[62] The convex hull of Alexandria included ≈120 000 compounds, and was by far the largest freely available. However, as the complete hull was not known, the calculated distances to the convex hull should be regarded as a lower limit.

For the machine learning part, the ALIGNN[63] model was trained using as targets, simultaneously, λ, $\omega_{\log}$ and T_c with the error for each property weighted equally, as these are the choices yielding the best results. The default hyperparameters were used. The final models can be downloaded from https://github.com/hyllios/utils/tree/main/models.

A few superconductivity simulations were performed with isotropic Eliashberg theory[53,54] including full ab initio Coulomb interactions. The Eliashberg α^2F function was computed using QUANTUM ESPRESSO[55,56] and density functional perturbation theory.[64,65] A converged momentum integration was performed by mapping the calculated electron–phonon matrix elements to a random set of 60 000 k-points accumulated on the Fermi surface.[66,67] All calculations were done using PBEsol pseudo potentials from the strict set of PseudoDojo[68] and a 100 Ry energy cutoff for the planewave expansion. A $16^3(8^3)$ k-grid(q-grid) was used for the zone sampling in calculating the dynamical matrices of Mg_2XH_6 and $LiPdH_2$, a $12^3(6^3)$ k-grid(q-grid) was used for the other systems in Table 3. Screening was computed[69] in the random phase approximation which was expected to be sufficiently accurate for this class of materials.[50] The response function was calculated with a G-vector cutoff of three atomic units and an energy window of two Hartrees. The k-grids for momentum integration of the Coulomb interaction converged to 10% in the value of μ, and ranged from 5^3 in Mg_2SrPdH_8 to 12^3 in $LiPdH_2$.

To verify the kinetic stability, NpT simulations were performed using VASP. Supercells with 270 atoms were used, obtained using the FIND_OPTIMAL_CELL_SHAPE routine from ASE.[70] The system was first thermalized during 2000 steps, during which the temperature was increased linearly from 0 to 150 K. Then 5000 steps were performed at constant temperature. The time step was set to 1 fs, and Langevin dynamics were used to model the thermostat and the barostat. For consistency, the PBEsol approximation was used for the exchange-correlation functional.

Supporting Information

Supporting Information is available from the Wiley Online Library or from the author.

Acknowledgements

T.F.T.C. acknowledges financial support from FCT - Fundação para a Ciência e Tecnologia, I.P. through the projects UIDB/04564/2020, UIDP/04564/2020 and CEECINST/00152/2018/CP1570/CT0006, with DOI identifiers 10.54499/UIDB/04564/2020, 10.54499/UIDP/04564/2020, and 10.54499/CEECINST/00152/2018/CP1570/CT0006, respectively. Computational resources provided by UC-LCA, funded by FCT I.P. under the project Advanced Computing Project 2022.15822.CPCA. M.A.L.M. acknowledges partial funding from Horizon Europe MSCA Doctoral network grant n.101073486, EUSpecLab, funded by the European Union, and from the Keele Foundation through the SuperC collaboration. Y.-W.F. and I.E. received funding from the European Research Council (ERC) under the European Union's Horizon 2020 research and innovation programme (Grant Agreement No. 802533) and acknowledge PRACE for awarding access to the EuroHPC supercomputer LUMI located in CSC's data center in Kajaani, Finland through EuroHPC Joint Undertaking (EHPC-REG-2022R03-090). I.E. also acknowledges funding from the Spanish Ministry of Science and Innovation (Grant No. PID2022-142861NA-I00) and the Department of Education, Universities

and Research of the Basque Government and the University of the Basque Country (Grant No. IT1527-22). The authors acknowledge enlightening discussions with the partners of the SuperC collaboration.

Open access funding enabled and organized by Projekt DEAL.

Conflict of Interest

The authors declare no conflict of interest.

Author Contributions

T.F.T.C. and M.A.L.M. performed the machine learning prediction and the preliminary analysis of the superconducting properties. A.S. performed the statistical analysis and the analysis of selected hydrides. All authors contributed to designing the research, interpreting the results, and writing of the manuscript.

Data Availability Statement

The data that support the findings of this study are available in the supplementary material of this article.

Received: March 6, 2024
Revised: May 17, 2024
Published online:

[1] L. Gao, Y. Y. Xue, F. Chen, Q. Xiong, R. L. Meng, D. Ramirez, C. W. Chu, J. H. Eggert, H. K. Mao, *Phys. Rev. B* **1994**, *50*, 4260.
[2] J. Nagamatsu, N. Nakagawa, T. Muranaka, Y. Zenitani, J. Akimitsu, *Nature* **2001**, *410*, 63.
[3] N. W. Ashcroft, *Phys. Rev. Lett.* **2004**, *92*, 187002.
[4] M. Somayazulu, M. Ahart, A. K. Mishra, Z. M. Geballe, M. Baldini, Y. Meng, V. V. Struzhkin, R. J. Hemley, *Phys. Rev. Lett.* **2019**, *122*, 027001.
[5] A. P. Drozdov, P. P. Kong, V. S. Minkov, S. P. Besedin, M. A. Kuzovnikov, S. Mozaffari, L. Balicas, F. F. Balakirev, D. E. Graf, V. B. Prakapenka, E. Greenberg, D. A. Knyazev, M. Tkacz, M. I. Eremets, *Nature* **2019**, *569*, 528.
[6] L. Ma, K. Wang, Y. Xie, X. Yang, Y. Wang, M. Zhou, H. Liu, X. Yu, Y. Zhao, H. Wang, G. Liu, Y. Ma, *Phys. Rev. Lett.* **2022**, *128*, 167001.
[7] P. Kong, V. S. Minkov, M. A. Kuzovnikov, A. P. Drozdov, S. P. Besedin, S. Mozaffari, L. Balicas, F. F. Balakirev, V. B. Prakapenka, S. Chariton, D. A. Knyazev, E. Greenberg, M. I. Eremets, *Nat. Commun.* **2021**, *12*, 1175.
[8] B. Stritzker, W. Buckel, *Z. Phys. A: Hadrons Nucl.* **1972**, *257*, 1.
[9] A. I. Kolesnikov, A. M. Balagurov, I. O. Bashkin, V. K. Fedotov, V. Y. Malyshev, G. M. Mironova, E. G. Ponyatovsky, *J. Phys.: Condens. Matter* **1993**, *5*, 5045.
[10] V. E. Antonov, I. T. Belash, O. V. Zharikov, A. I. Latynin, A. V. Pal'nichenko, *Fiz. Tverd. Tela* **1988**, *30*, 598.
[11] C. B. Satterthwaite, I. L. Toepke, *Phys. Rev. Lett.* **1970**, *25*, 741.
[12] J. M. Welter, F. J. Johnen, *Z. Physik B* **1977**, *27*, 227.
[13] M. A. Kuzovnikov, V. E. Antonov, V. I. Kulakov, V. D. Muzalevsky, N. S. Orlov, A. V. Palnichenko, Y. M. Shulga, *Phys. Rev. Mater.* **2023**, *7*, 024803.
[14] D. Wang, Y. Ding, H.-K. Mao, *Materials* **2021**, *14*, 7563.
[15] L. Boeri, R. Hennig, P. Hirschfeld, G. Profeta, A. Sanna, E. Zurek, W. E. Pickett, M. Amsler, R. Dias, M. I. Eremets, C. Heil, R. J. Hemley, H. Liu, Y. Ma, C. Pierleoni, A. N. Kolmogorov, N. Rybin, D. Novoselov, V. Anisimov, A. R. Oganov, C. J. Pickard, T. Bi, R. Arita, I. Errea, C. Pellegrini, R. Requist, E. K. U. Gross, E. R. Margine, S. R. Xie, Y. Quan, et al., *J. Phys.: Condens. Matter* **2022**, *34*, 183002.
[16] P. Duffer, D. M. Gualtieri, V. U. S. Rao, *Phys. Rev. Lett.* **1976**, *37*, 1410.
[17] B. Stritzker, *Z. Physik* **1974**, *268*, 261.
[18] R. Lucrezi, E. Kogler, S. Di Cataldo, M. Aichhorn, L. Boeri, C. Heil, *Commun. Phys.* **2023**, *6*, 73.
[19] Y.-W. Fang, Đ. Dangić, I. Errea, *Commun. Mater.* **2024**, *5*, 61.
[20] M. Gao, P.-J. Guo, H.-C. Yang, X.-W. Yan, F. Ma, Z.-Y. Lu, T. Xiang, H.-Q. Lin, *Phys. Rev. B* **2023**, *107*, 180501.
[21] K. Choudhary, K. Garrity, *npj Comput. Mater.* **2022**, *8*, 244.
[22] C. Tian, Y. He, Y. Zhu, J. Du, S. Liu, W. Guo, H. Zhong, J. Lu, X. Wang, J. Shi, *Adv. Funct. Mater.* **2023**, 34, 2304919.
[23] A. Sanna, T. F. T. Cerqueira, Y.-W. Fang, I. Errea, A. Ludwig, M. A. L. Marques, *npj Comput. Mater.* **2024**, *10*, 44.
[24] K. Dolui, L. J. Conway, C. Heil, T. A. Strobel, R. Prasankumar, C. J. Pickard, *Phys. Rev. Lett.* **2024**, *132*, 166001.
[25] J. Schmidt, N. Hoffmann, H.-C. Wang, P. Borlido, P. J. M. A. Carriço, T. F. T. Cerqueira, S. Botti, M. A. L. Marques, *Adv. Mater.* **2023**, *35*, 2210788.
[26] J. Schmidt, L. Pettersson, C. Verdozzi, S. Botti, M. A. L. Marques, *Sci. Adv.* **2021**, *7*, 7948.
[27] F. Zheng, Z. Zhang, S. Wu, Q. Lin, R. Wang, Y. Fang, C.-Z. Wang, V. Antropov, Y. Sun, K.-M. Ho, *Mater. Today Phys.* **2024**, *42*, 101374.
[28] Y. He, J. Lu, X. Wang, J. jie Shi, *Phys. Rev. B* **2023**, *108*, 054515.
[29] M. Kritikos, D. Nore´us, *J. Solid State Chem.* **1991**, *93*, 256.
[30] B. Huang, F. Bonhomme, P. Selvam, K. Yvon, P. Fischer, *J. Less-Common Met.* **1991**, *171*, 301.
[31] This nomenclature is relative to the band structure of the parent, semiconducting, compound.
[32] K. Ikeda, T. Sato, S.-i. Orimo, *Int. J. Mater. Res.* **2008**, *99*, 471.
[33] A. W. Overhauser, *Phys. Rev. B* **1987**, *35*, 411.
[34] C. E. Messer, J. C. Eastman, R. G. Mers, A. J. Maeland, *Inorg. Chem.* **1964**, *3*, 776.
[35] A. J. Maeland, W. D. Lahar, *Z. Phys. Chem.* **1993**, *179*, 181.
[36] A. Kamegawa, T. Abiko, M. Okada, *Mater. Sci. Forum* **2014**, *783–786*, 1686.
[37] W. Bronger, G. Ridder, *J. Alloys Compd.* **1994**, *210*, 53.
[38] S. Gao, T. Broux, S. Fujii, C. Tassel, K. Yamamoto, Y. Xiao, I. Oikawa, H. Takamura, H. Ubukata, Y. Watanabe, K. Fujii, M. Yashima, A. Kuwabara, Y. Uchimoto, H. Kageyama, *Nat. Commun.* **2021**, *12*, 201.
[39] H. Kohlmann, *J. Solid State Chem.* **2010**, *183*, 367.
[40] C. Jia, X. Li, Q. Li, J. Yang, *Phys. Rev. B* **2023**, *107*, L140404.
[41] M. Baaddi, R. Chami, O. Baalla, S. E. Quaoubi, A. Saadi, L. E. H. Omari, M. Chafi, *Environ. Sci. Pollut. Res.* **2023**.
[42] F. Belli, T. Novoa, J. Contreras-García, I. Errea, *Nat. Commun.* **2021**, *12*, 5381.
[43] Y. He, J. jie Shi, *Nano Lett.* **2023**, *23*, 8126.
[44] T. F. T. Cerqueira, A. Sanna, M. A. L. Marques, *Adv. Mater.* **2024**, *36*, 2307085.
[45] I. Errea, M. Calandra, F. Mauri, *Phys. Rev. Lett.* **2013**, *111*, 177002.
[46] H.-C. Wang, A. W. Huran, M. A. L. Marques, M. Nalabothula, L. Wirtz, Z. Romestan, A. H. Romero, *J. Phys. Chem. Lett.* **2023**, *14*, 9969.
[47] J. A. Flores-Livas, A. Sanna, E. K. U. Gross, *Eur. Phys. J. B* **2016**, *89*, 363.
[48] R. Akashi, M. Kawamura, S. Tsuneyuki, Y. Nomura, R. Arita, *Phys. Rev. B* **2015**, *91*, 224513.
[49] J. A. Flores-Livas, L. Boeri, A. Sanna, G. Profeta, R. Arita, M. Eremets, *Phys. Rep.* **2020**, *856*, 1.
[50] C. Pellegrini, C. Kukkonen, A. Sanna, *Phys. Rev. B* **2023**, *108*, 064511.
[51] S. Massidda, F. Bernardini, C. Bersier, A. Continenza, P. Cudazzo, A. Floris, H. Glawe, M. Monni, S. Pittalis, G. Profeta, A. Sanna, S. Sharma, E. K. U. Gross, *Supercond. Sci. Technol.* **2009**, *22*, 034006.
[52] D. J. Scalapino, J. R. Schrieffer, J. W. Wilkins, *Phys. Rev.* **1966**, *148*, 263.
[53] C. Pellegrini, R. Heid, A. Sanna, *J. Phys. Mater.* **2022**, *5*, 02 4007.
[54] A. Davydov, A. Sanna, C. Pellegrini, J. K. Dewhurst, S. Sharma, E. K. U. Gross, *Phys. Rev. B* **2020**, *102*, 214508.

[55] P. Giannozzi, S. Baroni, N. Bonini, M. Calandra, R. Car, C. Cavazzoni, D. Ceresoli, G. L. Chiarotti, M. Cococcioni, I. Dabo, A. D. Corso, S. de Gironcoli, S. Fabris, G. Fratesi, R. Gebauer, U. Gerstmann, C. Gougoussis, A. Kokalj, M. Lazzeri, L. Martin-Samos, N. Marzari, F. Mauri, R. Mazzarello, S. Paolini, A. Pasquarello, L. Paulatto, C. Sbraccia, S. Scandolo, G. Sclauzero, A. P. Seitsonen, et al., *J. Phys.: Condens. Matter* **2009**, *21*, 395502.
[56] P. Giannozzi, O. Andreussi, T. Brumme, O. Bunau, M. B. Nardelli, M. Calandra, R. Car, C. Cavazzoni, D. Ceresoli, M. Cococcioni, N. Colonna, I. Carnimeo, A. D. Corso, S. de Gironcoli, P. Delugas, R. A. DiStasio, A. Ferretti, A. Floris, G. Fratesi, G. Fugallo, R. Gebauer, U. Gerstmann, F. Giustino, T. Gorni, J. Jia, M. Kawamura, H.-Y. Ko, A. Kokalj, E. Küçükbenli, M. Lazzeri, et al., *J. Phys.: Condens. Matter* **2017**, *29*, 465901.
[57] J. P. Perdew, A. Ruzsinszky, G. I. Csonka, O. A. Vydrov, G. E. Scuseria, L. A. Constantin, X. Zhou, K. Burke, *Phys. Rev. Lett.* **2008**, *100*, 136406.
[58] J. Schmidt, N. Hoffmann, H.-C. Wang, P. Borlido, P. J. M. A. CarriÃ§o, T. F. T. Cerqueira, S. Botti, M. A. L. Marques, *Adv. Mater.* **2023**, *35*, 2210788.
[59] J. Schmidt, H.-C. Wang, T. F. T. Cerqueira, S. Botti, M. A. L. Marques, *Sci. Data* **2022**, *9*, 64.
[60] D. Zagorac, H. Müller, S. Ruehl, J. Zagorac, S. Rehme, *J. Appl. Crystallogr.* **2019**, *52*, 918.
[61] H. Glawe, A. Sanna, E. K. U. Gross, M. A. L. Marques, *New J. Phys.* **2016**, *18*, 093011.
[62] M. Evans, J. Bergsma, A. Merkys, C. Andersen, O. B. Andersson, D. Beltrán, E. Blokhin, T. M. Boland, R. Castañeda Balderas, K. Choudhary, A. Díaz Díaz, R. Domínguez García, H. Eckert, K. Eimre, M. E. Fuentes-Montero, A. M. Krajewski, J. J. Mortensen, J. M. Nápoles-Duarte, J. Pietryga, J. Qi, F. d. J. Trejo Carrillo, A. Vaitkus, J. Yu, A. Zettel, P. B. de Castro, J. M. Carlsson, T. F. T. Cerqueira, S. Divilov, H. Hajiyani, F. Hanke, et al., *Digital Discovery* **2024**.
[63] K. Choudhary, B. DeCost, *npj Comput. Mater.* **2021**, *7*, 185.
[64] S. Baroni, S. de Gironcoli, A. Dal Corso, P. Giannozzi, *Rev. Mod. Phys.* **2001**, *73*, 515.
[65] S. Baroni, P. Giannozzi, A. Testa, *Phys. Rev. Lett.* **1987**, *58*, 1861.
[66] A. Sanna, C. Pellegrini, E. Liebhaber, K. Rossnagel, K. J. Franke, E. K. U. Gross, *npj Quantum Mater.* **2022**, *7*, 6.
[67] M. A. L. Marques, M. Lüders, N. N. Lathiotakis, G. Profeta, A. Floris, L. Fast, A. Continenza, E. K. U. Gross, S. Massidda, *Phys. Rev. B* **2005**, *72*, 024546.
[68] M. van Setten, M. Giantomassi, E. Bousquet, M. Verstraete, D. Hamann, X. Gonze, G.-M. Rignanese, *Comput. Phys. Commun.* **2018**, *226*, 39.
[69] The Elk Code, http://elk.sourceforge.net/.
[70] A. H. Larsen, J. J. Mortensen, J. Blomqvist, I. E. Castelli, R. Christensen, M. Dułak, J. Friis, M. N. Groves, B. Hammer, C. Hargus, E. D. Hermes, P. C. Jennings, P. B. Jensen, J. Kermode, J. R. Kitchin, E. L. Kolsbjerg, J. Kubal, K. Kaasbjerg, S. Lysgaard, J. B. Maronsson, T. Maxson, T. Olsen, L. Pastewka, A. Peterson, C. Rostgaard, J. Schiøtz, O. Schütt, M. Strange, K. S. Thygesen, T. Vegge, et al., *J. Phys. Condens. Matter* **2017**, *29*, 273002.